Published in final edited form as:
J Am Chem Soc. 2010 October 13; 132(40): 14229–14238. doi:10.1021/ja106175q.

Potent, Highly Selective, and Orally Bioavailable *Gem*-Difluorinated Monocationic Inhibitors of Neuronal Nitric Oxide Synthase

Fengtian Xue[1,5], **Huiying Li**[2], **Silvia L. Delker**[2], **Jianguo Fang**[1], **Pavel Martásek**[3,4], **Linda J. Roman**[3], **Thomas L. Poulos**[2,*], and **Richard B. Silverman**[1,*]

[1] Department of Chemistry, Department of Biochemistry, Molecular Biology, and Cell Biology, Center for Molecular Innovation and Drug Discovery, Chemistry of Life Processes Institute, Northwestern University, 2145 Sheridan Road, Evanston, Illinois 60208-3113

[2] Departments of Molecular Biology and Biochemistry, Pharmaceutical Chemistry, and Chemistry, University of California, Irvine, California 92697-3900

[3] Department of Biochemistry, University of Texas Health Science Center, San Antonio, Texas

[4] Department of Pediatrics and Center for Applied Genomics, 1st School of Medicine, Charles University, Prague, Czech Republic

Abstract

In our efforts to discover neuronal isoform selective nitric oxide synthase (NOS) inhibitors we have developed a series of compounds containing a pyrrolidine ring with two stereogenic centers. The enantiomerically pure compounds, (*S*,*S*) vs. (*R*,*R*), exhibited two different binding orientations, with (*R*,*R*) inhibitors showing much better potency and selectivity. To improve the bioavailability of these inhibitors we have introduced a CF_2 moiety geminal to an amino group in the long tail of one of these inhibitors, which reduced its basicity, resulting in compounds with monocationic character under physiological pH conditions. Biological evaluations have led to a nNOS inhibitor with a K_i of 36 nM and high selectivity for nNOS over eNOS (3800-fold) and iNOS (1400-fold). MM-PBSA calculations indicated that the low pK_a NH is, at least, partially protonated when bound to the active site. A comparison of rat oral bioavailability of the difluorinated compound to the parent molecule shows 22% for the difluorinated compound versus essentially no oral bioavailability for the parent compound. This indicates that the goal of this research to make compounds with only one protonated nitrogen atom at physiological pH to allow for membrane permeability, but which can become protonated when bound to NOS, has been accomplished.

Introduction

Since its first discovery as the endothelium-derived relaxing factor (EDRF) in 1987,[1] nitric oxide (NO) has emerged as an important biological messenger involved in a wide variety of physiological functions as well as pathophysiological states. In living organisms, NO is produced by nitric oxide synthase (NOS), a homodimeric flavohemoprotein, through the oxidation of L-arginine to L-citrulline with NADPH and O_2 as cosubstrates.[2–4]

*Correspondence Authors: Richard B. Silverman, Department of Chemistry, Northwestern University, Agman@chem.northwestern.edu. Thomas L. Poulos, Department of Molecular Biology and Biochemistry, University of California, Irvine, poulos@uci.edu.
[5]*Present address:* Department of Chemistry, University of Louisiana at Lafayette, P.O. Box 44370, Lafayette, Louisiana 70504, USA

Supporting Information Available: Copies of complete spectroscopic data of compounds **9a**–**d**, **9f**, and **3a**–**f** are available.

To date, three distinct isoforms of mammalian NOS, namely neuronal NOS (nNOS), inducible NOS (iNOS), and endothelial NOS (eNOS), have been identified with high homology (>55%).[5] nNOS catalyzes the oxidation of L-arginine in the central nervous system, generating NO as a critical neurotransmitter.[6–7] Although normal activity of nNOS is important for neurotransmission, NO overproduction by nNOS has been shown to be associated with chronic neurodegenerative pathologies such as Parkinson's,[8] Alzheimer's,[9] and Huntington's diseases,[10] also with chronic headaches,[11] as well as neuronal damage in stroke.[12] iNOS, the isozyme of NOS that produces cytotoxic NO, is responsible for maintaining normal function of the immune system.[13] eNOS, on the other hand, regulates blood pressure. It has been shown experimentally that the reduced NO production by eNOS causes hypertension and atherosclerosis.[14] Therefore, selective inhibition of nNOS activity over its closely related isoforms, eNOS and iNOS, represents an exciting drug approach for the development of new therapeutic agents to treat neurodegenerative diseases.[5,15–16]

In our continuing efforts to develop nNOS selective inhibitors, we have discovered a pyrrolidine-based compound (**1**, Figure 1), which showed great potency (K_i = 15 nM) and excellent selectivity for nNOS over eNOS (2100-fold) and iNOS (630-fold).[17] However, further application of this compound as a drug candidate for neurodegenerative diseases is limited by its poor bioavailability.[18] The two positive charges of **1** at physiological pH, derived from the two basic amino (NH) groups, dramatically impair the ability of **1** to penetrate the blood brain barrier (BBB) by passive diffusion.[18] In addition, the benzylic position of the *m*-fluorophenylethyl substituent is susceptible to metabolic oxidation.[19]

To circumvent these problems, different strategies have been employed to improve the bioavailability of inhibitors by limiting the number of basic functional groups in **1**.[18,20,21] For example, by incorporating an electron-withdrawing group adjacent to the amino group in the hydrophobic tail, a series of low pK_a inhibitors were synthesized with monocationic or pseudo-monocationic characters at physiological pH.[20] Evaluation of these inhibitors led to the discovery of inhibitor **2**, with two fluorines substituted at the benzylic position of the *m*-fluorophenylethyl tail of **1**. The racemic mixture of **2** indicated good potency (K_i = 80 nM) and high selectivity for nNOS over both eNOS (1500-fold) and iNOS (650-fold). More importantly, it showed improved cell-membrane permeability compared to the parent compound **1**.[20] The CF_2 group is widely used in drug development because of its unique pharmacological properties.[22] For inhibitor **2**, the additional CF_2 group not only decreases the basicity of the adjacent amino group dramatically (pK_a ≈ 5.5), but also effectively blocks the potential metabolic oxidation at the benzylic position of the *m*-fluorophenyl ring.[19] We report here the structure-based design, synthesis, and biological evaluation of a series of enantiomerically pure inhibitors (**3a**–**f**) derived from inhibitor **2**, in an attempt to further improve the pharmacodynamic and pharmacokinetic properties of these inhibitors.

Results and Discussion

Chemistry

An improved synthesis of enantiomerically pure pyrrolidine core (**4a**–**b**) is shown in Scheme 1. First, racemic *trans*-alcohol **5** underwent a Mitsunobu reaction with (*S*)-(−)-camphanic acid as the nucleophile to produce two separable diastereomers (**6a** and **6b**) in excellent yields. Next, the ester in **6a** and **6b** was hydrolyzed in aqueous Na_2CO_3 to generate **4a** and **4b** in high yields.

As shown in Scheme 2, single enantiomer **4a** or **4b** was treated with NaH, and the resulting anion was allowed to react with allyl bromide to generate **7a** and **7b** in excellent yields. Ozonolysis of **7a** and **7b** using Zn dust as the reducing reagent yielded **8a** and **8b** in good yields. Aldehydes **8a** and **8b** were subjected to reductive amination reactions with different

ethanamines in the presence of $NaHB(OAc)_3$ to generate secondary amines, which were further protected by another Boc-protecting group to produce fully protected inhibitors **9a**–**d** in good yields. Next, the benzyl-protecting group was removed by catalytic hydrogenation using $Pd(OH)_2$ at 60 °C to provide **10a**–**d** in modest yields. Finally, the three Boc-protecting groups were removed at the same time in HCl to generate the final inhibitors (**3a**–**d**) in high yields.

The synthesis of inhibitor **3e** began with **9a** (Scheme 3). Catalytic hydrogenation of **9a** using $Pd(OH)_2$ at elevated temperature removed the benzyl-protecting group; when run for 48 h, the pyridinyl ring also was reduced to generate **10e** in modest yields. Then, the three Boc-protecting groups were removed in HCl to generate final inhibitor **3e** in high yields.

The synthesis of inhibitor **3f** is shown in Scheme 4. Reductive amination between aldehyde **8b** and 2,2-difluoro-2-(pyridin-2-yl)ethanamine generated a secondary amine, which was further protected by another Boc-protecting group to provide **9f** in good yields. Next, catalytic hydrogenation of **9f** removed the benzyl protecting group and also reduced the pyridinyl group adjacent to the CF_2 group to generate **10f** in modest yields. Finally, the three Boc-protecting groups were removed at the same time in HCl to generate inhibitor **3f** in high yields.

Crystal Structures of nNOS with 3a–3f Bound

Consistent with the binding preference of enantiomerically pure parental compound **1**,[23] the binding mode of these difluorinated derivatives is also dependent on the configuration around the two chiral centers, the 3′ and 4′ positions, of the pyrrolidine ring. While (*S*,*S*) inhibitor **3a** was found to bind with its aminopyridine moiety hydrogen bonded to the side chain of Glu592 in nNOS (Fig. 2A), (*R*,*R*) inhibitor **3b** adopted a 180° flipped binding mode with its aminopyridine making bifurcated hydrogen bonds with the heme propionate of pyrrole ring D (Fig. 2B). To make room for these new hydrogen bonds, the Tyr706 side chain rotates away and π-stacks against the aminopyridine ring of the inhibitor. The pyrrolidine nitrogen in **3b** also makes favorable hydrogen bonds with propionate A as well as the O4 atom of H_4B. In comparison, the pyrrolidine nitrogen in **3a** is only loosely hydrogen bonded to Glu592. The long, flexible linker extending from the pyrrolidine allows the fluorophenyl group in **3b** to reach the vicinity of Glu592 and to π-stack with the heme. The amino group vicinal to the CF_2 moiety points toward the Glu592 side chain, resulting in an alternate conformation of the carboxylate enabling a hydrogen bond to form between the amino nitrogen and the carboxylate oxygen (Fig. 2B). This alternate conformation of Glu592 was not observed in the structure of nNOS bound with **3a** because the tight bifurcated hydrogen bonds from the inhibitor aminopyridine to the carboxylate of Glu592 made an excellent match to the original conformation of the Glu side chain. The fit of the fluorophenyl group in **3b** near Glu592 is not ideal, and to avoid close van der Waals contacts with the inhibitor, Glu592 adopts the alternate conformation. In addition, the fluorophenyl tail of **3b** is disordered, as indicated by the weak electron density for this group. When only one conformation of the tail was modeled with the two fluorine atoms pointing away from the heme plane, strong negative difference density clustered around the fluorine atoms. Also, the electron density of the fluorophenyl ring could not be accounted for with only one ring orientation. The tail portion of **3b** was, therefore, modeled with two different conformations (0.6 and 0.4 occupancy) as shown in Fig. 2B. There also is a partially occupied site for a water molecule bridging between the heme propionate and the amino group in the tail portion of **3b** in the minor conformation. In contrast, the fluorophenyl ring in **3a** fits into a pocket formed by Met336, Leu337, and Tyr706 (Fig. 2A), but the density for **3a** is clear only up to the position of the two fluorine atoms thus precluding determination of the fluorophenyl ring orientation.

Inhibitor **3c** has its fluorine position in the phenyl ring changed from *meta* in **3b** to *para* in **3c**. Because the C-F bond is 1.34 Å, **3c** is at least 1.3 Å longer than **3b**. As a result, the *para*-F in **3c** makes a H-bond directly to the protein backbone amide (Gly586), while the *meta*-F of **3b** makes only a weak van der Waals contact with the protein (Fig. 3A). Because of the tighter contact of **3c**, the CF_2 moiety is forced into a downward conformation. The major conformation in **3b**, however, has the CF_2 moiety pointing upward. The downward conformation causes clashes between the CF_2 and heme propionate A, so the upward CF_2 conformation of **3b** represents a more relaxed fit in the active site, leading to higher potency.

Inhibitor **3d** is a derivative of **3b** and differs only by the absence of the fluorine on the phenyl ring. Its binding mode to nNOS is, therefore, almost identical to that of **3b** (Fig. 3B). Without the *meta*-fluorine the phenyl ring makes a looser contact with the hydrophobic pocket defined by Pro565, Val567, and Phe584. The phenyl tail portion in **3d** exhibits two alternate conformations similar to what is observed for **3b**.

Inhibitor **3e** has its aminopyridine ring partially reduced from that in **3d**, which has a negligible impact on the binding mode of the inhibitor compared to **3d** (Fig. 3C). The amino and the ring nitrogens remain planar and are still tightly hydrogen bonded to the heme propionate of pyrrole D, and the pyrrolidine nitrogen is hydrogen bonded to propionate A and H_4B. As in **3b** and **3d**, the phenyl tail in **3e** shows two conformations above the heme plane, and the Glu592 side chain also has two corresponding conformations.

Another (*S*,*S*) inhibitor, **3f**, is similar to **3a** except the fluorophenyl tail has been replaced by a piperidine ring. The binding of **3f** is similar to **3a** with its aminopyridine hydrogen bonded to the Glu592 side chain while the piperidine ring fits into the pocket of Met336, Leu337, and Tyr706 (Fig. 3D). The density for the tail portion is good only up to the CF_2 moiety with the piperidine partially disordered. Therefore, the orientation of the ring (position of nitrogen) is not well defined.

Crystal Structures of eNOS with 3b and 3f Bound

The eNOS structure bound with (*R*,*R*) inhibitor **3b** (Fig 4A) shows that it has adopted a 'flipped' binding mode, the same orientation as in nNOS. The Tyr477 side chain rotates farther out than in nNOS and, therefore, does not experience optimized π-stacking interactions with the aminopyridine of the inhibitor, as was observed in nNOS. Similar to what was seen in nNOS, the aminopyridine in **3b** makes bifurcated hydrogen bonds with the heme propionate of pyrrole ring D, while the pyrrolidine nitrogen makes favorable hydrogen bonds with propionate A as well as the O4 atom of H_4B (Fig. 4A). A hydrogen bond between the inhibitor amino group with alternate conformations for Glu363 also is observed. With the available density at the limited resolution only one conformation of the fluorophenyl tail portion can be modeled.

The binding of the (*S*,*S*) inhibitor **3f** in eNOS is similar to that in nNOS, with its aminopyridine hydrogen bonded to the Glu363 side chain (Fig. 4B) in the normal binding mode. The pyrrolidine nitrogen also hydrogen bonds with the conserved glutamate residue, but the density for the tail portion is good only up to the CF_2 moiety with the piperidine partially disordered. Therefore, the orientation of the ring (position of nitrogen) and the exact configuration of the puckered ring are not clear.

Inhibitory Assays and Structure-Based Evaluation

Inhibitors **3a**–**f** were evaluated for *in vitro* inhibition activities against three isozymes of NOSs including rat nNOS, bovine eNOS, and murine iNOS,[24] as summarized in Table 1. Compared to racemic lead compound **2**, (*S*,*S*) enantiomer **3a** is a weak inhibitor of nNOS with a K_i value of 390 nM, which is five-fold less potent than **2**. In addition, the selectivity

of this inhibitor for nNOS over eNOS and iNOS also decreases by 5-fold and 2-fold, respectively. The (*R*,*R*) enantiomer (**3b**), however, shows excellent potency for nNOS (K_i = 36 nM) and remarkable selectivity over eNOS (3800-fold) and iNOS (1400-fold). These results indicate that the chirality around the *cis*-chiral pyrrolidine core plays a key role in determining the potency and selectivity of inhibitors, as we have observed for another series of *trans*- or *cis*-chiral pyrrolidine inhibitors.[23] The potency and selectivity shown with racemic compound **2** can be attributed mainly to *(R,R)*-component **3b**. We now know that a large difference in binding affinity to nNOS between **3a** and **3b** originates from two different binding modes.[23] The flipped binding mode of **3b** relative to **3a** allows both the aminopyridine and pyrrolidine nitrogen atoms to make extensive hydrogen bonds with the heme and H_4B (Fig. 2B). In addition, as we have argued elsewhere,[23] the conformation of **3a** when bound to NOS places the pyrrolidine nitrogen atom very close to the aminopyridine, and because of electrostatic repulsion, this aminopyridine is only partially protonated. However, in the **3b** flipped orientation the aminopyridine is farther from the pyrrolidine nitrogen atom and remains fully protonated. Thus, the **3b** conformation provides greater electrostatic stabilization than the **3a** conformation, which accounts for the 10-fold lower K_i for **3b** than **3a**.

As a *p*-fluorophenyl derivative of **3b**, inhibitor **3c** shows a significant drop in potency for nNOS (K_i = 160 nM), which is 4.5-fold less potent than **3b**. More interestingly, **3c** loses 20-fold of selectivity over eNOS observed with **3b** by moving one single F atom from the *m*-position to the *p*-position of the phenyl tail. The new fluorine position leads to a 'difluoromethylene-down' binding mode of the inhibitor's phenyl tail. As a result, the hydrogen bond between the Glu592 side chain and the amino nitrogen in the tail seen in **3b** has been eliminated, which may explain the weaker potency and selectivity of **3c**.

Inhibitor **3d**, with the F atom removed from the phenyl tail, has restored good potency for nNOS (K_i = 85 nM) and high isozyme-selectivity (1500-fold over eNOS and 1000-fold over iNOS). This is because **3d** has retained the binding mode of **3b**. The only difference is that without a fluorine atom on the phenyl ring the van der Waals contacts to the protein (Pro565, Val567, and Phe584) are less optimal compared to that for **3b**. This results in a bit less potency and selectivity for **3d** than **3b**.

The amidino inhibitor **3e**, with the aromatic system of the aminopyridine fragment partially reduced, exhibits only a 2-fold drop in potency against nNOS compared to **3d**. Although π-π stacking of **3e** with Tyr706 should be greatly diminished relative to that with **3d**, the increased basicity of the amidine of **3e** over the aminopyridine of **3d** may compensate by producing a tighter electrostatic interaction with the heme propionate, resulting in only a factor of two difference for the K_i values of the these inhibitors. The removal of the aromatic system of the aminopyridine ring from inhibitor **3d** allows **3e** to bind more than 3-fold better to iNOS, thus exhibiting a much lower selectivity.

Finally, inhibitor **3f**, with an (*S*,*S*) configuration of the pyrrolidine core and a piperidinyl tail, showed poor inhibition activity and isozyme-selectivity. Both **3a** and **3f** have similar binding orientations and rather poor potency among the inhibitors reported in this work. This result emphasizes again that the chirality of the pyrrolidine core is the key to higher inhibitory activity with (*R*,*R*) inhibitors. In addition, a less polar aromatic ring such as the fluorophenyl group in **3a** seems to fit better into the pocket surrounded by Met336, Leu337, and Tyr706 in nNOS than does the polar piperidinyl ring in **3f**, and the π-stacking with the heme is lost in the case of **3f**. However, both **3a** and **3f** bind to eNOS with similar potency, possibly because of the smaller Val106 side chain in the pocket in eNOS compared to Met336 in nNOS.

The isoform selection shown for this series of inhibitors in Table 1 is not that straightforward to interpret based only on the structures presented here. For any one particular inhibitor among those reported in Table 1 the binding mode in eNOS is no different from that seen in nNOS. Similar to what we have discussed for another series of chiral pyrrolidine containing inhibitors,[23] one of the potential reasons for the isoform selectivity shown by **3b** is the difference in π-stacking interaction between the aminopyridine and Tyr706 in nNOS (or Tyr 477 in eNOS). We have consistently observed tighter interactions between this Tyr and the aminopyridine with nNOS complexed with inhibitors that adopt the **3b** flipped orientation.[23]

Calculations to Determine the Protonation State of Bound Inhibitors

The principal aim of this research was to lower the pK_a of one of the NH groups in the inhibitors, so that, at physiological pH, there would be effectively only one positive charge on the molecules, which should be acceptable for CNS penetration.[25] However, on the basis of past results, two positive charges are required for potency and isozyme selectivity. The aim was to find the appropriate pK_a so that once bound to NOS, the low pK_a NH would become protonated and could undergo the appropriate electrostatic interaction with a carboxylate.

In our initial work on flipped inhibitors,[23] we employed the Molecular Mechanics Poisson–Boltzmann/Surface Area (MM-PBSA)[26] computational method to calculate the free energy of binding of a series of aminopyridine inhibitors to nNOS and eNOS. We employed the empirical equation derived from Fig. 5, ΔGcalc = (PB-5.2874)/6.029, to obtain computed free energies. In our earlier work[23] we found that the best fits with ΔGexp resulted when the orientation of the inhibitor with the aminopyridine stacked over the heme (normal orientation) was assumed to be 50% protonated, while in the flipped orientation in which the aminopyridine interacts with the heme propionate, a +1 charge was assigned to the aminopyridine. The way partial charges were handled was to carry out the MM-PBSA calculations with a 0 or +1 charge and average the results. We carried out the same types of calculations with the difluorinated inhibitors used in this study, but the goal was to probe the state of protonation of the NH group whose p*Ka* has been lowered to ≈5.5 as a result of the fluorine atoms. The results of these calculations are shown in Table 2. With inhibitor **3b**, additional calculations were carried out because we observed two orientations in the nNOS active site. The best fit to ΔGexp results from assigning a full +1 charge to the aminopyridine in the “flipped” orientation and a +0.5 charge in the “normal” orientation and a +0.5 charge for the NH group in all the inhibitors independent of orientation. Our strategy for lowering the pK_a of the NH group was to decrease the total charge of the inhibitors in solution for better bioavailability but with the hope that they would become at least partially protonated once bound in the active site, where the nearby heme propionates and Glu592 might promote protonation. The calculations support this scenario and indicate that the NH group is partially protonated. This is reasonable because the NH group in these inhibitors, no matter which binding orientation, always H-bonds with one carboxylate and is within 4Å from another carboxylate (either the Glu592 side chain or the heme propionate).

Pharmacokinetic Data for 3b and (*R,R*)−1

The goal for insertion of two *gem*-fluorines into **1** was to lower the pK_a of one of the two basic nitrogen atoms to enhance metabolic stability and oral bioavailability but allow for potential reprotonation of that nitrogen atom once in the active site of nNOS. Pharmacokinetic properties of compound **3b** (the (*R,R*) isomer of the *gem*-difluorinated analogue corresponding to (*R,R*)−**1**) were compared to those of (*R,R*)−**1** to determine the effect of the difluorine substitution on pharmacokinetics. The in vivo compound half-life ($t_{1/2}$) for i.v. dosing at 1 mg/kg in rats (average of 3 rats) was 0.33 h for (*R,R*)−**1** and 7.5 h

for **3b**; the $t_{1/2}$ for oral dosing at 5 mg/kg was too low to measure for (*R*,*R*)−**1** and 3.7 h for **3b**; oral bioavailability for (*R*,*R*)−**1** was essentially zero and 22.2% for **3b**. It is apparent that the addition of the two fluorines has a remarkable effect on in vivo stability and oral bioavailability.

In summary, we have designed and synthesized a new series of selective nNOS inhibitors (**3a**–**f**) with monocationic character, and, therefore, potentially possessing better bioavailability. Biological evaluation of these new inhibitors based on crystal structures led to the discovery of inhibitor **3b**, which not only retains most of the inhibitory activity of lead compound **1**, but also shows remarkable selectivity for nNOS over both eNOS and iNOS. MM-PBSA calculations demonstrate that despite the pK_a of one of the nitrogen atoms in **3b** being 5.5, when bound to the active site, it becomes partially protonated for good binding. Whereas the in vivo half-life ($t_{1/2}$) and oral bioavailability in rats for the parent compound [(*R*,*R*)−**1**] are nil, when the two fluorines are added (**3b**), the $t_{1/2}$ rises to 10 h and oral bioavailability increases to 22%. This work represents a significant step forward toward the goal of developing drugs with therapeutic potential in the treatment of diseases caused by unregulated NO generation from nNOS.

Experimental Section

1. General Methods

All experiments were conducted under anhydrous conditions in an atmosphere of argon, using flame-dried apparatus and employing standard techniques in handling air-sensitive materials. All solvents were distilled and stored under an argon or nitrogen atmosphere before use. All reagents were used as received. Aqueous solutions of sodium bicarbonate, sodium chloride (brine), and ammonium chloride were saturated. Analytical thin layer chromatography was visualized by ultraviolet, ninhydrin, or phosphomolybdic acid (PMA). Flash column chromatography was carried out under a positive pressure of nitrogen. ^{1}H NMR spectra were recorded on 500 MHz spectrometers. Data are presented as follows: chemical shift (in ppm on the δ scale relative to δ = 0.00 ppm for the protons in TMS), integration, multiplicity (s = singlet, d = doublet, t = triplet, q = quartet, m = multiplet, br = broad), coupling constant (*J*/Hz). Coupling constants were taken directly from the spectra and are uncorrected. ^{13}C NMR spectra were recorded at 125 MHz, and all chemical shift values are reported in ppm on the δ scale, with an internal reference of δ 77.0 or 49.0 for $CDCl_3$ or MeOD, respectively. High-resolution mass spectra were measured on liquid chromatography/time-of-flight mass spectrometry (LC-TOF).

2. Preparation and Characterization of New Compounds

General Method A: Reductive Amination—To a solution of aldehyde **8a** or **8b** (0.1 mmol) in THF (3 mL) was added the ethanamine (0.2 mmol), followed by $NaHB(OAc)_3$ (0.12 mmol). The mixture was stirred at room temperature for an additional 3 h and then concentrated. The crude product was purified by flash column chromatography (EtOAc/hexanes, 2:1–4:1) to yield the corresponding secondary amines as colorless oils, which were used without further purification.

General Method B: Boc-protection—To a solution of the secondary amine (0.5 mmol) in MeOH (10 mL) was added $(Boc)_2O$ (164 mg, 0.75 mmol) and TEA (140 μL, 1.0 mmol). The reaction mixture was allowed to stir at room temperature for 30 min. The solvent was removed by rotary evaporation, and the resulting material was purified by flash column chromatography (EtOAc/hexanes, 1:4-1:2) to yield **9a**–**f** as colorless oils.

General Method C: Catalytic hydrogenation—To a solution of **9a**–**f** (0.2 mmol) in EtOH (20 mL) was added $Pd(OH)_2/C$ (100 mg). The reaction vessel was charged with H_2, heated at 60 °C for 24–48 h, then cooled to room temperature. The catalyst was removed by filtration, and the resulting solution was concentrated by rotary evaporation. The crude material was purified by flash column chromatography (EtOAc/hexanes, 1:4-1:2) to yield **10a**–**f** as white foamy solids.

General Method D: Boc-deprotection—To a solution of **10a**–**f** (50 μmol) in MeOH (0.5 mL) was added 6 N HCl (1.0 mL). The reaction mixture was allowed to stand at room temperature for 12 h. The solvent was removed by rotary evaporation. The crude product was recrystallized with cold diethyl ether to provide **3a**–**f** as pale yellow solids.

(9a)—9a was synthesized by general methods A and B using aldehyde **8b** as the starting material (60%): ^{1}H NMR (500 MHz, $CDCl_3$) δ 1.35–1.55 (m, 27H), 2.20–2.40 (s, 3H), 2.50–2.80 (m, 2H), 2.80–2.95 (m, 1H), 3.00–3.21 (m, 2H), 3.30–3.79 (m, 6H), 3.80–4.00 (m, 2H), 5.10–5.25 (s, 2H), 6.60–6.70 (br s, 1H), 7.00–7.30 (m, 8H), 7.31–7.60 (m, 2H); ^{13}C NMR (125 MHz, $CDCl_3$) δ 14.4, 21.2, 21.3, 27.8, 28.1, 28.4, 28.5, 28.7, 29.9, 34.8, 42.3, 42.9, 47.5, 47.7, 49.0, 49.4, 50.1, 50.4, 50.9, 60.6, 67.9, 76.9, 78.9, 79.3, 79.7, 79.8, 80.6, 81.4, 113.0, 113.1, 117.2, 117.5, 120.1, 121.4, 126.7, 126.8, 126.9, 127.0, 127.1, 127.2, 127.5, 127.6, 128.3, 128.5, 128.6, 130.4, 140.0 148.8, 154.1, 154.5, 154.9, 157.8, 161.5, 163.4; LCQ-MS ($M+H^+$) calcd for $C_{43}H_{58}F_3N_4O_7$ 799, found 799; LC-TOF ($M+H^+$) calcd for $C_{43}H_{58}F_3N_4O_7$ 799.4252, found 799.4258.

(9b)—9b was synthesized by general methods A and B using aldehyde **8a** as the starting material (58%): ^{1}H NMR (500 MHz, $CDCl_3$) δ 1.35–1.55 (m, 27H), 2.20–2.40 (s, 3H), 2.50–2.80 (m, 2H), 2.80–2.95 (m, 1H), 3.00–3.21 (m, 2H), 3.30–3.79 (m, 6H), 3.80–4.00 (m, 2H), 5.10–5.25 (s, 2H), 6.60–6.70 (br s, 1H), 7.00–7.30 (m, 8H), 7.31–7.60 (m, 2H); ^{13}C NMR (125 MHz, $CDCl_3$) δ 14.4, 21.2, 21.3, 27.8, 28.1, 28.4, 28.5, 28.7, 29.9, 34.8, 42.3, 42.9, 47.5, 47.7, 49.0, 49.4, 50.1, 50.4, 50.9, 60.6, 67.9, 76.9, 78.9, 79.3, 79.7, 79.8, 80.6, 81.4, 113.0, 113.1, 117.2, 117.5, 120.1, 121.4, 126.7, 126.8, 126.9, 127.0, 127.1, 127.2, 127.5, 127.6, 128.3, 128.5, 128.6, 130.4, 140.0 148.8, 154.1, 154.5, 154.9, 157.8, 161.5, 163.4; LCQ-MS ($M+H^+$) calcd for $C_{43}H_{58}F_3N_4O_7$ 799, found 799; LC-TOF ($M+H^+$) calcd for $C_{43}H_{58}F_3N_4O_7$ 799.4252, found 799.4248.

(9c)—9c was synthesized by general methods A and B using aldehyde **8a** as the starting material (48%): ^{1}H NMR (500 MHz, $CDCl_3$) δ 1.20–1.50 (m, 27H), 2.25–2.35 (m, 3H), 2.45–2.65 (m, 1H), 2.66–2.70 (m, 1H), 2.80–2.95 (m, 1H), 3.00–3.10 (m, 1H), 3.10–3.20 (m, 1H), 3.25–3.70 (m, 7H), 3.80–4.00 (m, 2H), 5.10–5.20 (m, 2H), 6.60–6.70 (m, 1H), 7.00–7.15 (m, 2H), 7.16–7.20 (m, 1H), 7.21–7.27 (m, 4H), 7.35–7.60 (m, 3H); ^{13}C NMR (125 MHz, $CDCl_3$) δ 13.7, 14.2, 19.1, 21.0, 21.1, 24.7, 27.91, 27.96, 28.01, 28.2, 28.3, 28.5, 30.6, 34.4, 34.5, 34.6, 42.0, 42.1, 42.6, 42.7, 47.4, 47.5, 47.6, 47.8, 48.8, 49.3, 49.9, 50.1, 50.3, 50.8, 53.4, 53.8, 54.0, 60.4, 64.4, 67.7, 67.8, 68.0, 78.7, 78.8, 79.1, 79.2, 79.3, 79.6, 80.3, 81.17, 81.22, 115.2, 115.4, 115.6, 115.7, 117.0, 117.1, 119.9, 126.5, 126.6, 126.9, 127.0, 127.5, 128.1, 131.5, 139.7, 139.8, 148.6, 153.9, 154.3, 154.4, 154.5, 154.6, 154.7, 154.8, 155.1, 157.4, 157.5, 157.6, 162.7, 164.6, 171.2; LC-TOF ($M+H^+$) calcd for $C_{43}H_{58}F_3N_4O_7$ 799.4258, found 799.4237.

(9d)—9d was synthesized by general methods A and B using aldehyde **8a** as the starting material (55%): ^{1}H NMR (500 MHz, $CDCl_3$) δ 1.20–1.50 (m, 27H), 2.25–2.35 (m, 3H), 2.45–2.65 (m, 1H), 2.66–2.71 (m, 1H), 2.80–2.95 (m, 1H), 3.00–3.10 (m, 1H), 3.10–3.20 (m, 1H), 3.25–3.70 (m, 7H), 3.80–4.00 (m, 2H), 5.10–5.20 (m, 2H), 6.60–6.70 (m, 1H), 7.00–7.60 (m, 12H); ^{13}C NMR (125 MHz, $CDCl_3$) δ 13.7, 14.2, 19.1, 21.0, 21.1, 24.7,

27.91, 27.96, 28.01, 28.2, 28.3, 28.5, 30.6, 34.4, 34.5, 34.6, 42.0, 42.1, 42.6, 42.7, 47.4, 47.5, 47.6, 47.8, 48.8, 49.3, 49.9, 50.1, 50.3, 50.8, 53.4, 53.8, 54.0, 60.4, 64.4, 67.7, 67.8, 68.0, 78.7, 78.8, 79.1, 79.2, 79.3, 79.6, 80.3, 81.17, 81.22, 115.2, 115.4, 115.6, 115.7, 117.0, 117.1, 119.9, 126.5, 126.6, 126.9, 127.0, 127.5, 128.1, 131.5, 139.7, 139.8, 148.6, 153.9, 154.3, 154.4, 154.5, 154.6, 154.7, 154.8, 155.1, 157.4, 157.5, 157.6, 162.7, 164.6, 171.2; LC-TOF ($M+H^+$) calcd for $C_{43}H_{59}F_2N_4O_7$ 781.4352, found 781.4366.

(9f)—9f was synthesized by general methods A and B using aldehyde **8b** as the starting material (55%): ^{1}H NMR (500 MHz, $CDCl_3$) δ 1.40–1.55 (m, 27H), 2.27–2.29 (m, 3H), 2.45–2.67 (m, 1H), 2.68–2.75 (m, 1H), 2.85–2.95 (m, 1H), 3.00–3.11 (m, 1H), 3.12–3.20 (m, 1H), 3.30–3.45 (m, 3H), 3.46–3.65 (m, 3H), 4.05–4.20 (m, 2H), 5.16 (s, 2H), 6.67 (s, 1H), 7.17–7.20 (m, 1H), 7.21–7.26 (m, 4H), 7.30–7.45 (m, 2H), 7.50–7.70 (m, 1H), 7.75–7.85 (m, 1H), 8.60–8.71 (m, 1H); ^{13}C NMR (125 MHz, $CDCl_3$) δ 14.2, 21.11, 21.13, 24.7, 28.0, 28.1, 28.2, 28.3, 28.5, 29.7, 34.4, 34.5, 36.6, 42.2, 42.6, 42.7, 47.6, 47.7, 48.0, 48.8, 49.2, 49.89, 49.92, 50.1, 50.2, 50.8, 60.4, 67.5, 67.6, 67.7, 78.7, 79.1, 79.6, 80.2, 81.1, 81.2, 117.0, 117.1, 120.0, 120.4, 120.5, 124.76, 124.84, 126.4, 126.5, 126.6, 126.9, 127.0, 128.06, 128.11, 136.9, 137.0, 139.8, 139.9, 148.5, 149.3, 149.5, 153.8, 154.3, 154.4, 154.5, 154.7, 155.0, 155.4, 157.7; LC-TOF ($M+H^+$) calcd for $C_{42}H_{58}F_2N_5O_7$ 782.4304, found 782.4299.

(3a)—3a was synthesized by general methods C and D using **9a** as the starting material (95%): ^{1}H NMR (500 MHz, D_2O) δ 2.29 (s, 3H), 2.78–2.81 (m, 2H), 2.95–3.05 (dd, *J* = 8.0, 15.0 Hz, 1H), 3.15–3.20 (t, *J* = 6.0, 1H), 3.31–3.35 (dd, *J* = 3.0, 13.0 Hz, 1H), 3.40–3.55 (m, 3H), 3.63–3.66 (d, *J* = 13.0 Hz, 1H), 3.71–3.79 (m, 1H), 3.87–3.95 (m, 3H), 4.24–4.26 (t, *J* = 3.0 Hz, 1H), 6.55 (s, 1H), 6.64 (s, 1H), 7.25–7.29 (dt, *J* = 2.5, 8.5 Hz, 1H), 7.34–7.36 (dd, *J* = 2.5, 14.0 Hz, 1H), 7.38–7.40 (dd, *J* = 2.5, 8.0 Hz, 1H), 7.49–7.52 (dd, *J* = 6.0, 8.0 Hz, 1H); ^{13}C NMR (125 MHz, D_2O) δ 21.0, 29.1, 41.3, 47.0, 47.5, 49.2, 51.5, 51.7, 51.9, 63.6, 78.3, 110.4, 112.3, 112.5, 114.0, 118.2, 118.4, 118.6, 121.0, 131.2, 131.3, 134.2, 145.5, 153.9, 158.1, 161.4, 163.3; LC-TOF ($M+H^+$) calcd for $C_{21}H_{28}F_3N_4O$ 409.2215, found 409.2226.

(3b)—3b was synthesized by general methods C and D using **9b** as the starting material (100%): ^{1}H NMR (500 MHz, D_2O) δ 2.29 (s, 3H), 2.78–2.81 (m, 2H), 2.95–3.05 (dd, *J* = 8.0, 15.0 Hz, 1H), 3.15–3.20 (t, *J* = 6.0, 1H), 3.31–3.35 (dd, *J* = 3.0, 13.0 Hz, 1H), 3.40–3.55 (m, 3H), 3.63–3.66 (d, *J* = 13.0 Hz, 1H), 3.71–3.79 (m, 1H), 3.87–3.95 (m, 3H), 4.24–4.26 (t, *J* = 3.0 Hz, 1H), 6.55 (s, 1H), 6.64 (s, 1H), 7.25–7.29 (dt, *J* = 2.5, 8.5 Hz, 1H), 7.34–7.36 (dd, *J* = 2.5, 14.0 Hz, 1H), 7.38–7.40 (dd, *J* = 2.5, 8.0 Hz, 1H), 7.49–7.52 (dd, *J* = 6.0, 8.0 Hz, 1H); ^{13}C NMR (125 MHz, D_2O) δ 21.0, 29.1, 41.3, 47.0, 47.5, 49.2, 51.5, 51.7, 51.9, 63.6, 78.3, 110.4, 112.3, 112.5, 114.0, 118.2, 118.4, 118.6, 121.0, 131.2, 131.3, 134.2, 145.5, 153.9, 158.1, 161.4, 163.3; LC-TOF ($M+H^+$) calcd for $C_{21}H_{28}F_3N_4O$ 409.2215, found 409.2223.

(3c)—3c was synthesized by general methods C and D using **9c** as the starting material (95%): ^{1}H NMR (500 MHz, D_2O) δ 2.30 (s, 3H), 2.78–2.81 (m, 2H), 2.95–3.05 (dd, *J* = 8.0, 15.0 Hz, 1H), 3.15–3.20 (t, *J* = 6.0, 1H), 3.31–3.35 (dd, *J* = 3.0, 13.0 Hz, 1H), 3.40–3.55 (m, 3H), 3.63–3.66 (d, *J* = 13.0 Hz, 1H), 3.71–3.79 (m, 1H), 3.87–3.95 (m, 3H), 4.24–4.26 (t, *J* = 3.0 Hz, 1H), 6.55 (s, 1H), 6.64 (s, 1H), 7.21–7.25 (dd, *J* = 8.5, 8.5 Hz, 2H), 7.59–7.62 (dd, *J* = 5.0, 8.5 Hz, 2H); ^{13}C NMR (125 MHz, D_2O) δ 21.0, 29.0, 41.3, 47.0, 47.4, 49.2, 51.7, 51.9, 51.9, 63.6, 78.3, 110.4, 113.9, 116.0, 116.1, 118.7, 127.42, 127.47, 127.55, 127.59, 145.5, 153.9, 158.1; LC-TOF ($M+H^+$) calcd for $C_{21}H_{28}F_3N_4O$ 409.2215, found 409.2230.

(3d)—3d was synthesized by general methods C and D using **9d** as the starting material (95%): ^{1}H NMR (500 MHz, D_2O) δ 2.30 (s, 3H), 2.73–2.84 (m, 2H), 2.95–3.05 (dd, *J* = 8.5,

15.0 Hz, 1H), 3.10–3.20 (t, *J* = 6.0, 1H), 3.31–3.35 (dd, *J* = 3.0, 13.5 Hz, 1H), 3.40–3.55 (m, 3H), 3.63–3.66 (d, *J* = 13.5 Hz, 1H), 3.71–3.79 (m, 1H), 3.87–3.95 (m, 3H), 4.24–4.26 (t, *J* = 3.0 Hz, 1H), 6.55 (s, 1H), 6.64 (s, 1H), 7.45–7.65 (m, 5H); ^{13}C NMR (125 MHz, D_2O) δ 21.0, 29.0, 41.3, 47.0, 47.4, 49.2, 51.6, 51.8, 52.0, 63.6, 78.2, 110.4, 113.9, 119.0, 120.9, 124.81, 124.86, 124.91, 129.1, 131.6, 131.9, 132.1, 145.5, 153.9, 158.1;; LC-TOF ($M+H^+$) calcd for $C_{21}H_{29}F_2N_4O$ 391.2309, found 391.2337.

(3e)—3e was synthesized by general methods C and D using **9e** as the starting material (96%): ^{1}H NMR (500 MHz, D_2O) δ 0.85–0.95 (d, *J* = 2.5, 3H), 1.45–1.55 (m, 1H), 1.61–1.70 (m, 1H), 1.71–1.97 (m, 3H), 2.00–2.10 (m, 1H), 2.35–2.45 (m, 1H), 2.46–2.57 (m, 1H), 2.90–3.00 (t, *J* = 6.0, 1H), 3.16–3.21 (m, 1H), 3.30–3.50 (m, 4H), 3.51–3.60 (d, *J* = 13.5 Hz, 1H), 3.61–3.70 (m, 1H), 3.75–3.90 (m, 3H), 4.14s-4.16 (t, *J* = 3.0 Hz, 1H), 7.45–7.65 (m, 5H); ^{13}C NMR (125 MHz, D_2O) δ 17.5, 17.6, 18.2, 26.8, 27.2, 27.3, 32.6, 32.9, 40.0, 40.2, 48.3, 48.9, 49.1, 49.6, 50.6, 52.2, 58.8, 65.2, 79.9, 80.0, 115.4, 115.6, 116.8, 117.0, 126.0, 132.1, 132.2, 140.2, 163.1, 165.0, 168.4; LC-TOF ($M+H^+$) calcd for $C_{21}H_{33}F_2N_4O$ 395.2622, found 395.2633.

(3f)—3f was synthesized by general methods C and D using **9f** as the starting material (100%): ^{1}H NMR (500 MHz, D_2O) δ 1.40–1.50 (m, 1H), 1.51–1.60 (m, 2H), 1.79–1.90 (m, 2H), 1.91–1.98 (d, *J* = 13.5 Hz, 1H), 2.20 (s, 3H), 2.65–2.75 (m, 1H), 2.79–2.85 (m, 1H), 2.94–2.96 (d, *J* = 7.5 Hz, 1H), 2.97–3.00 (m, 1H), 3.07–3.12 (dd, *J* = 11.5, 11.5 Hz, 1H), 3.20–3.26 (dd, *J* = 0.5, 13.0 Hz, 1H), 3.31–3.47 (m, 4H), 3.52–3.55 (d, *J* = 13.5 Hz, 1H), 3.61–3.64 (m, 1H), 3.74–3.82 (m, 5H), 4.11 (s, 1H), 6.52 (s, 1H), 6.57 (s, 1H); ^{13}C NMR (125 MHz, D_2O) δ 20.4, 21.05, 21.06, 22.4, 28.95, 29.01, 41.48, 41.51, 45.1, 47.0, 48.08, 48.14, 49.4, 57.7, 63.7, 63.9, 78.3, 78.4, 110.4, 114.09, 114.12, 145.7, 153.9, 158.1; LC-TOF ($M+H^+$) calcd for $C_{20}H_{34}F_2N_5O$ 398.2742, found 398.2726.

Enzyme Assays

The three isozymes, murine macrophage iNOS, rat nNOS, and bovine eNOS, were recombinant enzymes, overexpressed (in *E. coli*) and isolated as reported.[27] IC_{50} values for inhibitors **3a**–**f** were measured for the three different isoforms of NOS using *L*-arginine as a substrate. The formation of nitric oxide was measured using a hemoglobin capture assay described previously.[24] All NOS isozymes were assayed at room temperature in a 100 mM Hepes buffer (pH 7.4) containing 10 μM L-arginine, 1.6 mM $CaCl_2$, 11.6 μg/mL calmodulin, 100 μM DTT, 100 μM NADPH, 6.5 μM H_4B, 3.0 μM oxyhemoglobin (for iNOS assays, no Ca^{2+} and calmodulin were added). The assay was initiated by the addition of enzyme, and the initial rates of the enzymatic reactions were determined by monitoring the formation of NO-hemoglobin complex at 401 nm for 60 sec. The corresponding K_i values of inhibitors were calculated from the IC_{50} values using equation 1 with known K_m values (rat nNOS, 1.3 μM; iNOS, 8.3 μM; eNOS, 1.7 μM).

$$K_i = IC_{50} / (1 + [S]/K_m) \quad (1)$$

Inhibitor Complex Crystal Preparation

The nNOS or eNOS heme domain protein used for crystallographic studies were produced by limited trypsin digest from the corresponding full length enzymes and further purified through a Superdex 200 gel filtration column (GE Healthcare) as described previously.[28] The enzyme-inhibitor complex crystals were obtained by soaking rather than co-crystallization as reported in the earlier structural work.[29] The nNOS heme domain at 7–9 mg/mL containing 20 mM histidine or the eNOS heme domain at 20 mg/mL with 2 mM

imidazole were used for the sitting drop vapor diffusion crystallization setup under the conditions reported before.[28,30] Fresh crystals (1–2 day old) were first passed stepwise through cryo-protectant solutions described[28,30] and then soaked with 10 mM inhibitor for 4–6 h at 4 °C before being mounted on nylon loops and flash cooled by plunging into liquid nitrogen. Crystals were stored in liquid nitrogen until data collection.

X-ray Diffraction Data Collection, Processing, and Structure Refinement

The cryogenic (100K) X-ray diffraction data were collected remotely at various beamlines at Stanford Synchrotron Radiation Lightsource through the data collection control software Blu-Ice[31] and the crystal mounting robot. Raw data frames were indexed, integrated, and scaled using HKL2000.[32] Typically, each data set consisted of 90 to 100 degree of data with a 0.5 degree frame width for both nNOS and eNOS crystals because of their identical orthorhombic $P2_12_12_1$ space group symmetry.

The binding of inhibitors was detected by the initial difference Fourier maps calculated with REFMAC.[33] The inhibitor molecules were then modeled in O[34] or COOT[35] and refined using REFMAC. Water molecules were added in REFMAC and checked by COOT. The TLS[36] protocol was implemented in the final stage of refinements with each subunit as one TLS group. The refined structures were validated in COOT before deposition to RCSB protein data bank. The crystallographic data collection and structure refinement statistics are summarized in Table 3 with PDB accession codes included.

Molecular Mechanics Poisson–Boltzmann/SurfaceA (MM-PBSA) Method for Free Energy of Binding of Inhibitors

The MM-PBSA method[26] as implemented in Amber 9.0 was used to compute the free energy of binding of inhibitors to NOS and was previously described in detail.[23] To briefly summarize, the free energies of 10 different aminopyridine inhibitors-NOS complexes were calculated from a single energy minimized structure starting from the known crystal structures described in our previous work.[23] A plot of the resulting computed free energy (PB) vs ΔGexp, obtained from experimental K_i values. The empirical equation derived from Fig. 5, ΔGcalc = (PB-5.2874)/6.029, was used to calculate free energies of binding for the inhibitors used in the present study.

Pharmacokinetic Data—All pharmacokinetic results were obtained by LC-MS-MS analysis and calculation of PK parameters using WinNonlin software at BioDuro, Inc., Shanghai, China.

Supplementary Material

Refer to Web version on PubMed Central for supplementary material.

Acknowledgments

The authors are grateful for financial support from the National Institutes of Health (GM49725 to RBS and GM57353 to TLP). We thank Dr. Bettie Sue Siler Masters (NIH grant GM52419, with whose laboratory P.M. and L.J.R. are affiliated). B.S.S.M. also is grateful to the Welch Foundation for a Robert A. Welch Distinguished Professorship in Chemistry (AQ0012). P.M. is supported by grants 0021620806 and 1M0520 from MSMT of the Czech Republic. We also thank the staff at SSRL for their assistance during the remote X-ray diffraction data collections.

References

1. Palmer RMJ, Ferrige AG, Moncada S. Nature. 1987; 327:524. [PubMed: 3495737]
2. Marletta MA. J Biol Chem. 1993; 268:12231. [PubMed: 7685338]

3. Marletta MA. Cell. 1994; 78:927. [PubMed: 7522970]
4. Griffith OW, Stuehr DJ. Annu Rev Physiol. 1995; 57:707. [PubMed: 7539994]
5. Alderton WK, Cooper CE, Knowles RG. Biochem J. 2001; 357:593. [PubMed: 11463332]
6. Hall AV, Antoniou H, Wang Y, Cheung AH, Arbus AM, Olson SL, Lu WC, Kau CL, Marsden PA. J Biol Chem. 1994; 269:33082. [PubMed: 7528745]
7. Wang Y, Newton DC, Marsden PA. Crit Rev Neurobiol. 1999; 13:21. [PubMed: 10223522]
8. Zhang L, Dawson VL, Dawson TM. Pharmacol Ther. 2006; 109:33. [PubMed: 16005074]
9. Dorheim MA, Tracey WR, Pollock JS, Grammas P. Biochem Biophys Res Commun. 1994; 205:659. [PubMed: 7528015]
10. Norris PJ, Waldvogel HJ, Faull RLM, Love DR, Emson PC. Neuronsicence. 1996; 72:1037.
11. Ashina M. Exp Opin Pharmacother. 2002; 3:395.
12. Sims NR, Anderson MF. Neurochem Int. 2002; 40:511. [PubMed: 11850108]
13. Hobbs AJ, Higgs A, Moncada S. Annu Rev Pharmacol. 1999; 39:191.
14. Dawson VL, Dawson TM, London ED, Bredt DS, Snyner SH. Proc Natl Acad Sci. 1991; 88:6368. [PubMed: 1648740]
15. Southan GJ, Szabo C. Biochem Pharmacol. 1996; 51:383. [PubMed: 8619882]
16. Babu BR, Griffith OW. Curr Opin Chem Biol. 1998; 2:491. [PubMed: 9736922]
17. Ji H, Li H, Martásek P, Roman LJ, Poulos TL, Silverman RB. J Med Chem. 2009; 52(3):779. [PubMed: 19125620]
18. Lawton GR, Ranaivo HR, Wing LK, Ji H, Xue F, Martesek P, Roman LJ, Watterson DM, Silverman RB. Bioorg Med Chem. 2009; 17:2371. [PubMed: 19268602]
19. Silverman, RB. The Organic Chemistry of Drug Design and Drug Action. 2. Elsevier; 2004.
20. Xue F, Fang J, Lewis WW, Martásek P, Roman LJ, Silverman RB. Bioorg Med Chem Lett. 2010; 20:554. [PubMed: 19963381]
21. Xue F, Huang J, Ji H, Fang J, Li H, Martásek P, Roman LJ, Poulos TP, Silverman RB. Bioorg Med Chem. 2010; 18:6526. [PubMed: 20673724]
22. Smart BE. J Fluorine Chem. 2001; 109:3.
23. Delker DL, Ji H, Li H, Jamal J, Fang J, Xue X, Silverman RB, Poulos TL. J Am Chem Soc. 2010; 132:5437. [PubMed: 20337441]
24. Hevel JM, Marletta MA. Method Enzymol. 1994; 233:250.
25. Kerns, EH.; Di, L. Drug-like Properties: Concepts, Structure Design and Methods. Academic Press; Amsterdam: 2008. p. 130
26. Massova I, Kollman PA. J Am Chem Soc. 1999:8133.
27. (a) Hevel JM, White KA, Marletta M. J Biol Chem. 1991; 266(34):22789. [PubMed: 1720773] (b) Roman LJ, Sheta EA, Martásek P, Gross SS, Liu Q, Masters BSS. Proc Natl Acad Sci USA. 1995; 92(18):8428. [PubMed: 7545302] (c) Martasek P, Liu Q, Roman LJ, Gross SS, Sessa WC, Masters BSS. Biochem Biophys Res Commun. 1996; 219(2):359. [PubMed: 8604992]
28. Li H, Shimizu H, Flinspach M, Jamal J, Yang W, Xian M, Cai T, Wen EZ, Jia Q, Wang PG, Poulos TL. Biochemistry. 2002; 41:13868. [PubMed: 12437343]
29. Flinspach ML, Li H, Jamal J, Yang W, Huang H, Hah JM, Gomez-Vidal JA, Litzinger EA, Silverman RB, Poulos TL. Nat Struct Mol Biol. 2004; 11:54. [PubMed: 14718923]
30. Raman CS, Li H, Martasek P, Kral V, Masters BS, Poulos TL. Cell. 1998; 95:939. [PubMed: 9875848]
31. McPhillips TM, McPhillips SE, Chiu HJ, Cohen AE, Deacon AM, Ellis PJ, Garman E, Gonzalez A, Sauter NK, Phizackerley RP, Soltis SM, Kuhn P. J Synchrotron Radiat. 2002; 9:401. [PubMed: 12409628]
32. Otwinowski Z, Minor W. Methods Enzymol. 1997; 276:307.
33. Murshudov GN, Vagin AA, Dodson EJ. Acta Cryst. 1997; D53:240.
34. Jones TA, Zou JY, Cowan SW, Kjeldgaarrd M. Acta cryst. 1991; A47:110.
35. Emsley P, Cowtan K. Acta Cryst. 2004; D60:2126.
36. Winn MD, Isupov MN, Murshudov GN. Acta Cryst. 2001; D57:122.

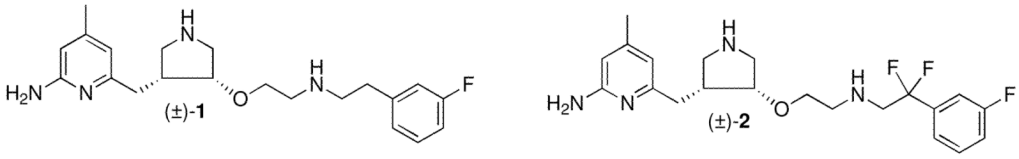

Figure 1.
Chemical structures of **1** and **2**

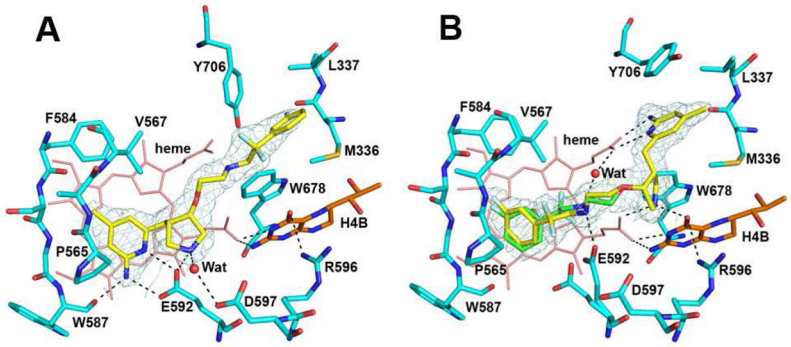

Figure 2.

The nNOS active site with inhibitor **3a** (A) or **3b** (B) bound. The sigmaA weighted 2Fo − Fc density for inhibitor is also shown at contour level of 1 σ. Hydrogen bonds are depicted with dashed lines. The atomic color schemes are: N, blue; O, red; S, yellow; F, light cyan. Alternate conformations for **3b** (yellow and green) and E592 were observed. Figures 2, 3, and 4 were prepared with PyMol (http://www.pymol.org)

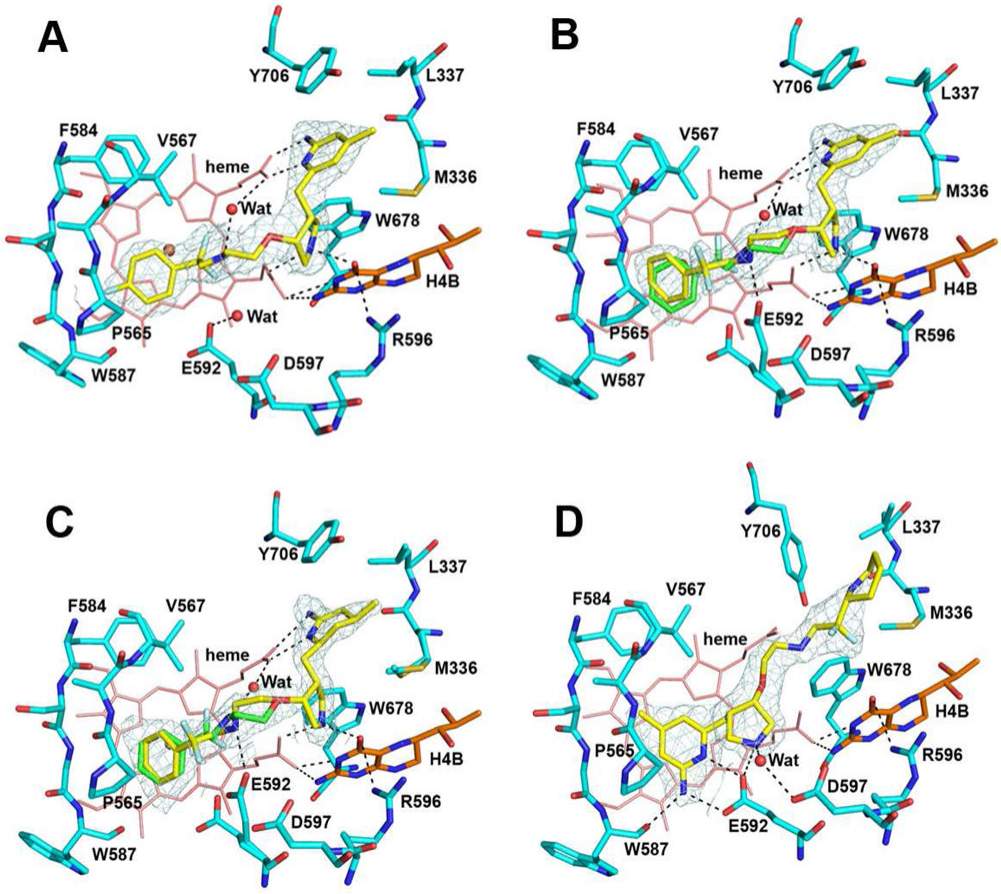

Figure 3.

The nNOS active site with **3c** (A), **3d** (B), **3e** (C), or **3f** (D) bound. Around each inhibitor is the sigmaA weighted 2Fo − Fc density contoured at 1 σ. Major hydrogen bonds are depicted with dashed lines. The same atomic color schemes as in Figure 1 are used. Note the alternate conformations for E592 occur when the inhibitor shows multiple conformations in the nNOS-**3d** or nNOS-**3e** structure.

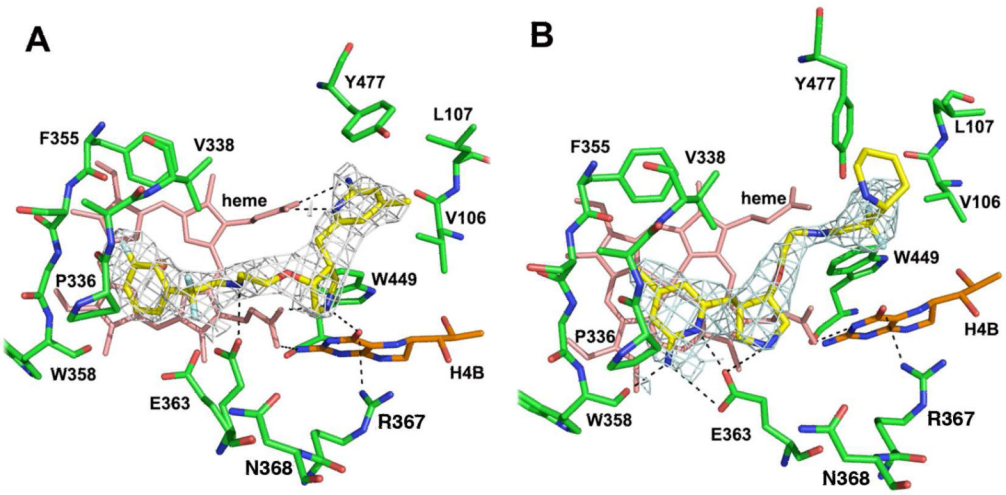

Figure 4.

The eNOS active site with **3b** (A) and **3f** (B) bound. Around each inhibitor is the sigmaA weighted 2Fo − Fc density contoured at 1 σ. Major hydrogen bonds are depicted with dashed lines. The same atomic color schemes as that in Figure 2 are used. As observed with nNOS, alternate conformations for Glu363 occur in the eNOS-**3b** structure.

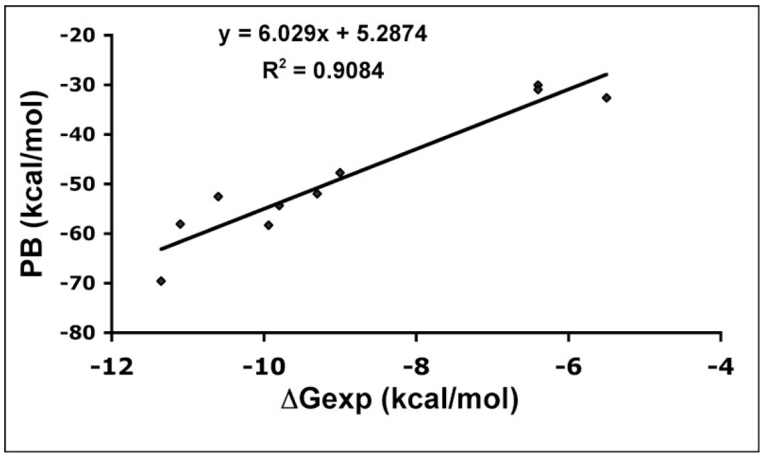

Figure 5.
Plot of the computed free energy (PB) vs experimental free energy (ΔGexp) obtained from K_i values.

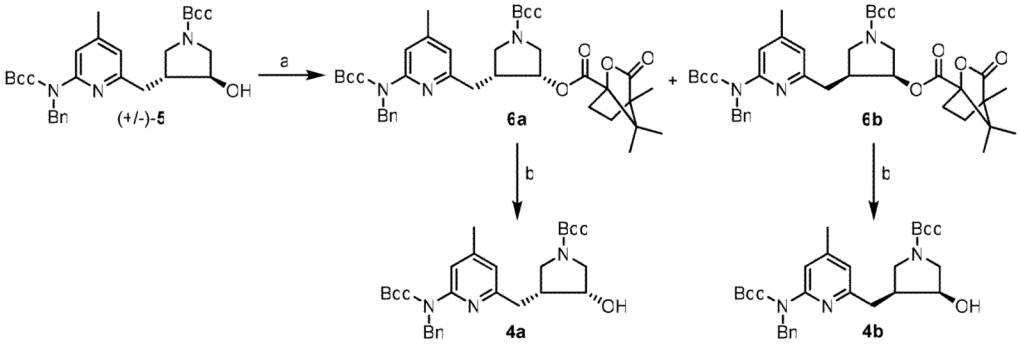

Scheme 1.
Synthesis of **4a**–**b**[a]
[a] Reagents and conditions: (a) (*S*)-(−)-camphanic acid, PPh_3, DIAD, rt, 16 h, 95%; (d) Na_2CO_3, rt, 4 h, 95%.

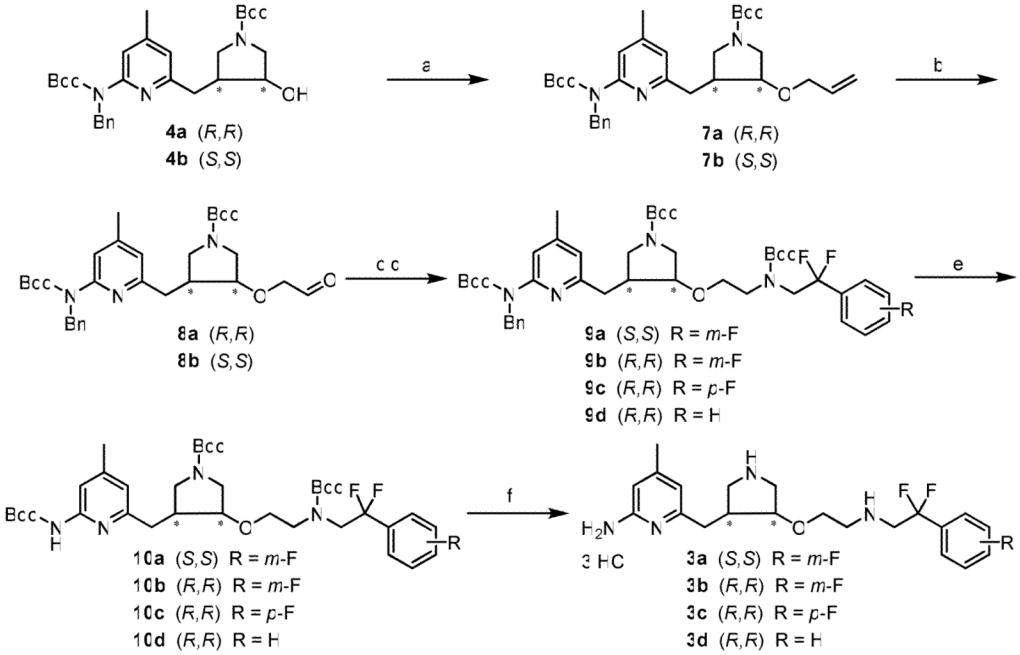

Scheme 2.

Synthesis of **3a**–**d**[a]

[a] Reagents and conditions: (a) (i) NaH, (ii) allyl bromide, rt, 1 h, 96%; (b) O_3, −78 ° C, (ii) Zn, −78 °C to rt, 2 h, 81%; (c) (i) ethanamines, THF, r.t., 5 min, (ii) $NaHB(OAc)_3$, r.t., 3 h; (d) $(Boc)_2O$, Et_3N, MeOH, r.t., 3 h, 48–60% for two steps; (e) $Pd(OH)_2/C$, H_2, EtOH, 60 ° C, 30 h, 45–60%; (f) 6 N HCl/MeOH (2:1), r.t., 16 h, 95–100%.

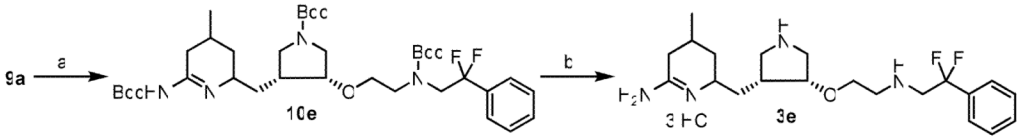

Scheme 3.

Synthesis of **3e**[a]

[a] Reagents and conditions: (a) $Pd(OH)_2/C$, H_2, EtOH, 60 ° C, 48 h, 55%; (d) 6 N HCl/MeOH (2:1), r.t., 16 h, 96%.

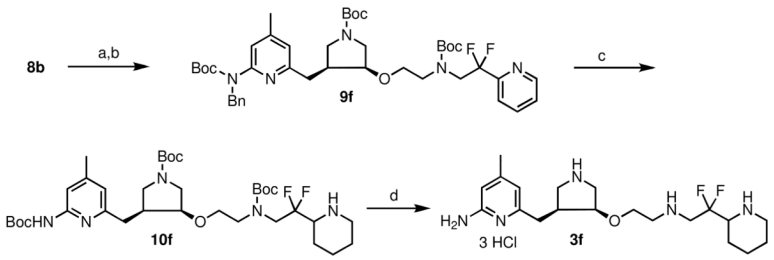

Scheme 4.

Synthesis of **3f**[a]

[a] Reagents and conditions: (a) (i) 2,2-difluoro-2-(pyridin-2-yl)ethanamine, THF, r.t., 5 min, (ii) $NaHB(OAc)_3$, r.t., 3 h; (b) $(Boc)_2O$, Et_3N, MeOH, r.t., 3 h, 55% for two steps; (c) $Pd(OH)_2/C$, H_2, EtOH, 60 ° C, 30 h, 60%; (d) 2 N HCl/MeOH (1:1), r.t., 16 h, 100%.

Table 1

K_i[a] values of inhibitors for rat nNOS, bovine eNOS, and murine iNOS.

Compound	nNOS (μM)	eNOS (μM)	iNOS (μM)	selectivity[b]	
				n/e	n/i
2	0.080	120	52	1500	650
3a	0.390	110	130	280	330
3b	0.036	140	51	3800	1400
3c	0.160	31	190	190	1200
3d	0.085	130	85	1500	1000
3e	0.170	130	26	770	150
3f	2.70	64	450	24	170

[a]The K_i values were calculated based on the directly measured IC_{50} values, which represent at least duplicate measurements with standard deviations of ±10%.

[b]The ratio of K_i (eNOS or iNOS) to K_i (nNOS).

Table 2

Calculated free energies for three inhibitors used in this study assuming different charges. For **3b** two different conformations of the inhibitor were observed in the crystal structure referred to here as conformations A and B.

inhibitor	charge on pyrrolidine	charge on NH	charge on amino pyridine	PB	ΔGcalc	ΔGexp	ΔΔG
3a	1	1	1	−77.3	−13.70	−8.8	4.90
3a	1	1	0	−47.66	−8.78	−8.8	0.018
3a	1	0	0	−18.75	−3.99	−8.8	4.81
	average				**−8.82**	**−8.8**	**0.022**
3c	1	0	1	−24.02	−4.86	−7.92	3.06
3c	1	1	1	−55.9	−10.15	−7.92	2.23
	average				**−7.50**	**−7.92**	**0.42**
3b A	1	1	1	−66.03	−11.83	−10.2	1.63
3b B	1	1	1	−82.7	−14.59	−10.2	4.39
3b A	1	0	1	−45.02	−8.34	−10.2	1.86
3b B	1	0	1	−36.25	−6.89	−10.2	3.31
	average				**−10.41**	**−10.2**	**0.21**

J Am Chem Soc. Author manuscript; available in PMC 2011 October 13.

Table 3

Crystallographic data collection and refinement statistics

Data set[1]	nNOS-3a	nNOS-3b	nNOS-3c	nNOS-3d
Data collection				
PDB code	3NLV	3NLX	3NLY	3NLZ
Space group	$P2_12_12_1$	$P2_12_12_1$	$P2_12_12_1$	$P2_12_12_1$
Cell dimensions				
a, *b*, *c* (Å)	52.3, 111.7, 164.4	52.3, 111.5, 164.4	51.8, 111.2, 164.1	51.9, 110.4, 164.0
Resolution (Å)	2.10 (2.14-2.10)	1.87 (1.90-1.87)	2.00 (2.03-2.00)	1.92 (1.95-1.92)
R_{sym} or R_{merge}	0.080 (0.59)	0.053 (0.36)	0.078 (0.40)	0.050 (0.32)
$I/\sigma I$	9.1 (2.2)	13.5 (3.9)	7.6 (1.8)	11.5 (2.6)
No. unique reflections	56,857	79,054	63,439	73,017
Completeness (%)	99.4 (99.5)	98.2 (96.5)	96.7 (80.9)	99.4 (89.8)
Redundancy	5.6 (2.9)	4.1 (4.1)	3.9 (3.1)	4.1 (3.6)
Refinement				
Resolution (Å)	2.10	1.87	2.00	1.92
No. reflections used	54,011	75,069	60,245	69,320
R_{work}/R_{free}	0.175/0.211	0.178/0.209	0.201/0.249	0.173/0.210
No. atoms				
Protein	6,671	6,689	6,676	6,707
Ligand/ion	187	223	190	217
Water	434	479	190	417
R.m.s. deviations				
Bond lengths (Å)	0.013	0.012	0.015	0.013
Bond angles (°)	1.325	1.390	1.554	1.456

Data set[1]	nNOS-3e	nNOS-3f	eNOS-3b	eNOS-3f
Data collection				
PDB code	3NM0	3NLW	3NLU	3NLT
Space group	$P2_12_12_1$	$P2_12_12_1$	$P2_12_12_1$	$P2_12_12_1$
Cell dimensions				
a, *b*, *c* (Å)	52.1, 110.9, 164.2	52.2, 111.4, 164.7	58.0, 107.0, 156.9	57.9, 106.9, 157.0
Resolution (Å)	1.81 (1.84-1.81)	2.10 (2.14-2.10)	2.65 (2.70-2.65)	2.75 (2.80-2.75)
R_{sym} or R_{merge}	0.048 (0.38)	0.069 (0.55)	0.121(0.58)	0.103 (0.65)
$I/\sigma I$	12.1 (2.7)	9.2 (2.4)	9.7 (1.9)	12.4 (1.9)
No. unique reflections	86,908	56,364	28,366	25,670
Completeness (%)	99.0 (92.5)	99.2 (100.0)	97.3 (99.1)	95.6 (94.4)
Redundancy	4.0 (3.8)	4.1 (4.1)	3.7 (3.7)	3.9 (4.0)
Refinement				
Resolution (Å)	1.81	2.10	2.65	2.74
No. reflections used	82,532	53,523	26,957	24,379
R_{work}/R_{free}[2]	0.178/0.209	0.171/0.207	0.185/0.254	0.186/0.262

Data set[1]	nNOS-3e	nNOS-3f	eNOS-3b	eNOS-3f
No. atoms				
Protein	6,716	6,676	6,451	6,419
Ligand/ion	217	185	197	195
Water	459	319	111	60
R.m.s. deviations				
Bond lengths (Å)	0.013	0.013	0.014	0.014
Bond angles (°)	1.360	1.347	1.502	1.519

[1] See Schemes 2, 3, and 4 for nomenclature and chemical formula of inhibitors.

[2] R_{free} was calculated with the 5% of reflections set aside throughout the refinement. For each NOS isoform the set of reflections for the R_{free} calculation were kept the same for all data sets according to those used in the data of the starting model.